Available online at www.sciencedirect.com
ScienceDirect
Journal of Non-Crystalline Solids 354 (2008) 1322–1326
JOURNAL OF NON-CRYSTALLINE SOLIDS
www.elsevier.com/locate/jnoncrysol

Optical and structural properties of new chalcohalide glasses

M. Guignard [a], V. Nazabal [a,*], A. Moreac [b], S. Cherukulappurath [c], G. Boudebs [c], H. Zeghlache [d], G. Martinelli [d], Y. Quiquempois [d], F. Smektala [a], J.-L. Adam [a]

[a] UMR CNRS 6512 Laboratoire Verres et Céramiques, Institut de Chimie de Rennes, Université Rennes 1, 35 042 Rennes cedex, France
[b] UMR CNRS 6626, Université, GMCM, Rennes 1, 35042 Rennes Cedex, France
[c] UMR CNRS 6136 Laboratoire POMA, Université d'Angers, 49045 Angers, France
[d] UMR CNRS 8523 Laboratoire de PhLAM, Université Lille 1, 59 655 Villeneuve d'Ascq cedex, France

Available online 3 December 2007

Abstract

New class of chalcohalide glasses has been prepared in the GeS_2–In_2S_3–CsI system with regard to their potential non-linear properties. The study of glass-forming region was undertaken to select glassy compositions, which present high non-linear (NL) optical properties with a low two-photon absorption. Thermal analyses, structural examination by Raman spectroscopy, non-linear optical measurements were investigated as a function of CsI contents. Introduction of CsI has shifted the band-gap edge towards the blue region of the absorption optical spectrum and therefore has limited the two-photon absorption. Their NL refractive index n_2 are 60 times higher than silica glasses without any NL absorption. Moreover, second harmonic signal was observed in thermally poled samples similar to silica glass. However, this second order non-linearity is not temporally stable.

PACS: 42.70.Km; 42.65.Ky; 78.30.−j

Keywords: Chalcohalides; Non-linear optics; Raman Spectroscopy; Short-range order

1. Introduction

Studying chalcogenide glasses is of great interest due to their interesting properties: large infrared spectral range of transparency, low phonon energy, photosensitivity, high linear and non-linear refractive indexes and the possibility to perform optical waveguides [1]. Therefore, these materials present great potential for the conception of electrooptic modulators in the IR spectral region [2]. For example, they can present third order non-linear refractive index n_2 more than 800 times higher than silica glasses [3]. However, these Se and As-containing glasses also exhibit a large non-linear absorption at the telecommunication wavelength of 1.55 μm which reduces their efficiency. The purpose of this study is focused on the selection of glasses which present high non-linear (NL) optical properties with a low two-photon absorption. The expected band-gap edge shift of chalcohalide glasses to shorter wavelengths could reduce the two-photon absorption compared to those of selenium-based chalcogenide glasses. In previous studies, the effects of halogens or halides addition on glass-forming ability, structural organization or band-gap energy were mainly investigated in As–S, Ge–S, Sb–S and Ge–Ga–S-based chalcogenide glasses [4–8]. However, there was only a few investigation on indium-containing glass formers among the chalcohalide systems [9,10]. In this present work, the incorporation of cesium iodide in the Ge–In–S system, earlier explored by Boncheva–Mladenova and Ivanova and lately by several authors, was investigated [11–16]. Non-linear optical properties of some compositions whose band-gap edge was shifted towards the blue region of the spectrum to avoid two-photon absorption were reported in this article.

* Corresponding author. Tel.: +33 2 2323 5748; fax: +33 2 2323 5611.
E-mail address: virginie.nazabal@univ-rennes1.fr (V. Nazabal).

0022-3093/$ - see front matter © 2007 Elsevier B.V. All rights reserved.
doi:10.1016/j.jnoncrysol.2007.01.104

2. Experimental methods

Samples were prepared by melting the raw materials (Ge, In, S and CsI, all of 5 N purity) in a silica tube under vacuum in a rocking furnace. The glass transition temperature T_g and crystallization temperature T_x (onset crystallization) were investigated by differential scanning calorimetry (DSC, heating rate of 10 °C min^{-1}) in order to establish the glass-forming region and the thermal stability of the GeS_2–In_2S_3–CsI glasses.

Thermal expansion coefficients (α) were obtained by measuring the expansion of cylinders of about 5 mm in length (heating rate of 2 °C min^{-1}). Density was determined in CCl_4 by using the Archimede's principle.

Visible-IR spectra were recorded from 0.4 to 15 μm. Linear refractive indexes were measured at 633, 1304 and 1540 nm by means of prism coupling technique applied to samples with a thickness of about 1 mm. Non-linear (NL) characterization of three samples was performed using the Z-scan technique at 1064 nm and 15 ps pulsewidth. Thermal poling was realized under N_2 gas and carried out at 70 °C below T_g. Thermal equilibrium duration before applying the voltage was fixed to 1 h and the applied voltage was 4 kV. The samples were poled during 30 min, then they were cooled down to room temperature and the high voltage was removed. They were characterized using a classical Maker fringes (MF) experiment with a pump beam of $\lambda = 1904$ nm [17].

Raman investigations were carried out to control the influence of CsI incorporation on the sulfide glass network organization. Raman spectra of $(100-x)GeS_2$–xIn_2S_3 ($x = 20$, 22.5, 25, 28.5) and $(80-x)GeS_2$–$20In_2S_3$–xCsI ($x = 10, 20, 30, 40$) glasses were recorded using a Ti:sapphire tunable laser (Spectra-Physics 3900S, exciting line at 775 nm for this study) coupled to a confocal micro-Raman triple spectrometer (DILOR XY500) in backscattering configuration; the typical resolution was 2.5 cm^{-1}. All spectra were recorded at room temperature. In order to minimize the effect of the boson peak at low frequencies, reduced Raman intensities were calculated, defined as $I_{red}(\omega) = I(\omega).\omega/[n(\omega)+1]$ [18]. The term I(ω) represents experimental Raman intensity at ω pulsation and $n(\omega)$ is the Bose-Einstein factor, defined as $n(\omega) = (\exp[(\hbar\omega/k_BT) - 1])^{-1}$. Reduced Raman spectra are decomposed into a set of pseudo-Voigt and the results of fitting are represented in Fig. 3.

3. Results

3.1. Glass-forming region

Fig. 1 represents the glass-forming region obtained by quenching the tubes – containing 7 g of materials – from 850 °C to room temperature in cold water. To synthesize binary samples combining GeS_2 with In_2S_3 needed for the structural investigation, smaller batches (2 g) were quenched from 920 °C to room temperature at a cooling rate of approximately 50 °C/s. In these conditions, the maximum content of In_2S_3 obtained for was about 25 mol% in agreement with Boncheva–Mladenova and Ivanova. Addition of CsI to GeS_2–In_2S_3 binary system reveals a wide vitreous domain compare to binary systems, up to 50 mol% of CsI. The composition of the glasses was controlled by EDS and only a slight lack of sulfur and an excess of germanium are always observed in the range of 1–2%. However, these differences are constants from a synthesis to another confirming the reproducibility of the elaboration process.

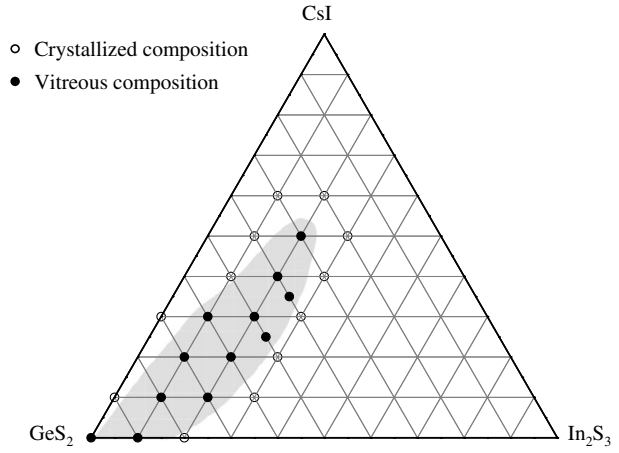

Fig. 1. Glass-forming region in GeS_2–In_2S_3–CsI system.

3.2. Physical properties

As shown in Table 1, glass transition temperature T_g are comprised in a range of 220–340 °C depending on the composition. For some compositions, no crystallization was observed during the DSC analysis up to 450 °C. That shows a good thermal stability. These compositions were quenched in air and annealed at a temperature close to T_g to be cut and polished to study their optical properties. A decrease of T_g and an increase of thermal expansion coefficient and volumic weight were observed when the CsI amount increased. The compositional dependence of glass density was likely due to the substitution of GeS_2 by heavier CsI compound. The infrared optical transmission spectra revealed the presence of absorption bands at 2.9, 4.0 and 6.2 μm assigned, respectively, to O–H, S–H and H_2O vibrations. The moderate increase of the intensity of these

Table 1
Characteristic temperatures T_g and T_x, volumic weight (ρ) and thermal expansion coefficient (α)

Compositions (mol%)			$T_g \pm 2$ (°C)	$\rho \pm 0.01$ (g cm^{-3})	$\alpha \times 10^7 \pm 5 \times 10^7$ (K^{-1})
GeS_2	In_2S_3	CsI			
80	10	10	341	3.16	165
70	20	10	337	3.37	161
70	10	20	336	3.28	225
60	20	20	321	3.46	196
50	20	30	302	3.54	237
40	20	40	266	3.62	271

vibration modes when the samples were immersed in water that demonstrates their slight sensitivity to moisture.

3.3. Optical properties

The obtained glasses were yellowish and their optical transmission in the visible range begins from 0.44 to 0.50 μm depending on the composition. Their long-wavelength absorption edge was measured at approximately 11 μm for glasses of 1 mm thick. The introduction of CsI in $(80-x)GeS_2$–$20In_2S_3$–$xCsI$ glasses, with $x = 0$–40 mol%, leads to a decrease of the band-gap wavelength from 550 to 440 nm. The linear (n) and non-linear (n_2) refractive indices are given in Table 2. A decrease of the refractive index n is observed when the CsI amount increases whereas third order non-linear refractive indices n_2 measured for three different compositions are similar in the detection limit. For these chalco-iodide glasses no significant non-linear absorption was observed ($\beta < 0.5$ cm/GW).

Second harmonic generation (SHG) was observed in two glasses of different composition after a thermal poling treatment. Fig. 2 shows the second harmonic signals (SHS) recorded after the poling treatment. Different MF patterns were obtained. In the case of the $50GeS_2$–$20In_2S_3$–30CsI glass, the SHS increases when the absolute value of the pump beam angle of incidence increases and reaches a maximum around 60°. Then, it decreases to zero due to the Fresnel losses at high angle. Its intensity is similar to SHS intensity in a thermally poled Infrasil silica glass. In the case of the $70GeS_2$–$20In_2S_3$–10CsI glass, we can observe large and well contrasted fringes or overmodulations on the MF pattern and the SHS intensity is about ten times lower than the SHS intensity for the $50GeS_2$–$20In_2S_3$–30CsI glass. However, SHS disappeared less than 24 h after the poling treatment for both glasses.

Table 2
Band-gap wavelength (λ), linear refractive index (n) and non-linear refractive index (n_2)

Compositions (mol%)			$\lambda \pm 5$ (nm)	$n \pm 0.001$			$n_2 \times 10^{18}$ ($m^2\ W^{-1}$) ± 20%
GeS_2	In_2S_3	CsI		633 (nm)	1304 (nm)	1550 (nm)	
70	20	10	502	2.204	2.125	2.120	1.6
60	20	20	472	2.130	2.062	2.055	1.4
50	20	30	447	2.068	2.004	2.000	1.6

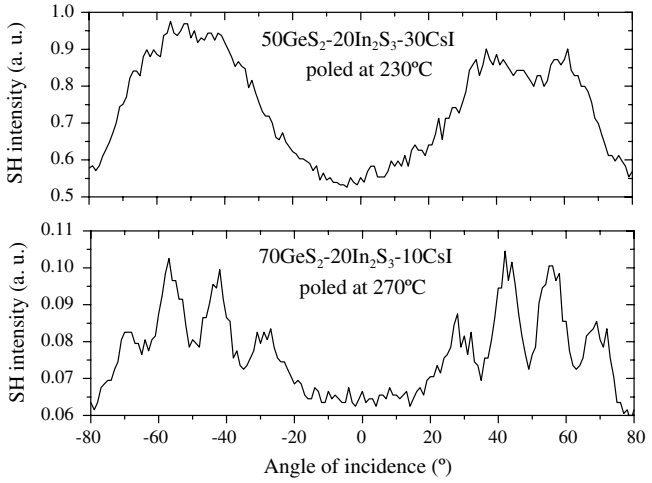

Fig. 2. MF obtained for two different glasses.

3.4. Raman spectroscopy

To minimize the effect of the boson peak at low frequencies, reduced Raman intensities were calculated, defined as $I_{red}(\omega) = I(\omega)\cdot\omega/[n(\omega)+1]$ [18]. The term $I(\omega)$ represents the experimental Raman intensity at ω pulsation, and $n(\omega)$ is the Bose-Einstein factor, defined as $n(\omega) = (\exp[(\hbar\omega/kT)-1]^{-1}$, where h is reduced Planck's constant. Reduced Raman spectra for $(80-x)GeS_2$–$20In_2S_3$–$xCsI$ ($0 \leqslant x \leqslant 40$) reported in Fig. 3 are dominated by a broad band between 270 and 430 cm^{-1} resulting from the overlap of several bands. The three characteristic bands – reported on the Raman spectrum of GeS_2 of glassy GeS_2 [19] – are clearly observed at 342, 369 and 433 cm^{-1} for the $80GeS_2$–$20In_2S_3$ spectrum (a). The first band at 342 cm^{-1} has been associated with the $\nu_1(A_1)$ symmetric stretching modes of $[GeS_4]$ tetrahedra. The two other peaks, usually related to the medium range order structure of GeS_2, have been associated with the $\nu_1^c(A_1^c)$ usually called 'companion peak', whose origin remains controversial, and to the vibration of Ge–S bonds in tetrahedral units linked by corners, respectively [19,20]. The introduction of indium leads to appearance of new bands, in the Raman spectrum of Ge–In–S glass, in the region between 210 and 260 cm^{-1}, of about 152 cm^{-1} and 308 cm^{-1}. When the In/Ge ratio increases, the intensity of the bands at 242 and 308 cm^{-1} rises unlike that at 343 cm^{-1} associated to the decrease of $[GeS_4]$ in favour of Indium structural unit. As it does not

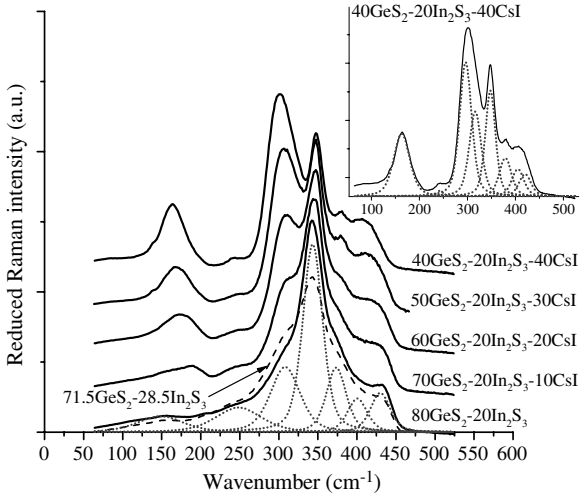

Fig. 3. Raman spectra of $(80-x)GeS_2$–$20In_2S_3$–$xCsI$ glasses with $x = 0$, $x = 10$, $x = 20$, $x = 30$ and $x = 40$ in mole percentage and of $71.5GeS_2$–$28.5In_2S_3$ glass (dashed curve). The Raman spectrum of $40GeS_2$–$20In_2S_3$–40CsI is plotted in the corner.

exist on the Raman spectrum of GeS_2 glass, the band observed at 148 cm^{-1} is probably related to a bending vibration mode involving indium structural entities. By analogy with the ternary glasses system Ge–Ga–S [21], it is reasonable to assume that in S-deficient (1–x)GeS_2–xIn_2S_3 glasses, Indium will occupy preferentially tetrahedral sites. This assumption is reinforced by X-ray absorption fine structure spectroscopy for which In atoms are found to be tetrahedrally coordinated by four sulfur nearest neighbours in the sulfur-excess glass and by 3.6 sulfur+0.4 germanium neighbours in the stoechiometric and S-deficient glass. Thus, the band at 308 cm^{-1} is assigned to the In–S vibration mode in [InS_4] tetrahedral [15,16]. In addition, the Indium introduction favors the formation of metal–metal bonds to offset the sulfur deficit of these glasses. Thus, the broad band in the range of 210–260 cm^{-1} may be related to the formation of Ge–In and Ge–Ge. According to EXAFS studies, In–In homopolar bonds are less probable being the expression of the absence of indium cluster with the respect of chemical order even for metal–metal bonding [14]. Nevertheless, this wide band centred at 242 cm^{-1} has also been related to the presence of [InS_6] octahedral sites [15,16] due to the presence of two really intense bands at 242 cm^{-1} and 308 cm^{-1} beta-In_2S_3 spinel-like structure where In atoms occupy octahedral and a part of tetrahedral sites [22]. Due to the increase of In/Ge ratio with the gradual introduction of CsI in the binary sample, the expected decrease of the bands in the range of 340–430 cm^{-1} related to the vibrations of the [GeS_4] entities is observed. The deconvolution of the broad band rising at about 300 cm^{-1} reveals two contributions. They can be related to an overlap of the In–S vibration mode in [InS_4] tetrahedra and probably in [$InS_{4-x}I_x$] entities since vibration of [$GeS_{4-x}I_x$] entities were recorded in the range of 250–260 cm^{-1}, 220–230 cm^{-1}, 200 cm^{-1} in Ge–S–I glasses [21,23]. The growth of vibration modes observed between 120 and 200 cm^{-1} centered at 164 cm^{-1} can be attributed to the formation of mixed entities of [$InS_{4-x}I_x$], rich in iodine as $CsInI_4$ at 141 cm^{-1} [24], and [$GeS_{4-x}I_x$] highlighted in the glasses system Ge–S–I for $x > 1$ and recorded for GeI_4 molecular units ($V_1 = 159$ cm^{-1}) [25]. The introduction of CsI significantly decreases the proportion of entities like ethane entities $S_3Ge(In)$–$Ge(In)S_3$ in the range of vibration between 220–260 cm^{-1}. This analysis is supported by the increase of average coordination number around metal atoms (3.19 to 3.69). Thus, we can expect a growth of the band associated to the mode of vibration of [InS_4] and [$InS_{4-x}I_x$] tetrahedra relatively to [GeS_4] tetrahedra in the event that [$GeS_{4-x}I_x$] and [$InS_{4-x}I_x$]structural entities are formed at the expense of entities $S_3Ge(In)$–$(In)GeS_3$ considering the vibration mode positions of each mixte structural units.

4. Discussion

The evolution of the glass transition temperature T_g and of the thermal expansion coefficient α with the increase of the CsI amount reveals the decrease of the dimensionality of the network, in agreement with Raman spectroscopy analyses in $(80 - x)GeS_2$–$20In_2S_3$–$xCsI$ $(0 \leqslant x \leqslant 40)$ glasses. The [GeS_4] structural entities should be progressively replaced by [InS_4] and [$InS_{(4-x)}I_x$/Cs] groups breaking the In_2S_3–GeS_2 covalent network with a smaller number of metal–metal bonds and a higher number of terminating iodine atoms. The probable formation of [$InS_{(4-x)}I_x$] groups indicates the ability of In atoms to form complex anions similar to the case of Ga atoms in GeS_2–Ga_2S_3 system [7]. The vibrational band assignment for mixed units [$Ge(In)S_{4-x}I_x$] remains delicate deserving further study.

Addition of cesium iodide in the binary glass GeS_2–In_2S_3 results in a decrease of the band-gap wavelength towards the blue region of the visible spectrum, this phenomenon can be explained by the electronegativity of the iodine atoms which reduces the electron delocalization in the glass network, and consequently, increases the band-gap energy. Although the introduction of halogenide generally decreases the NL refractive index of chalcogenide glasses, the conservation of a significant hyperpolarizability is facilitated by the presence of iodine. Therefore, their NL refractive index n_2 are still 60 times higher than silica glasses without any NL absorption.

According to results obtained in Ge_{25} chalcogenide glass [26], SHG in thermally poled samples can be attributed to the presence of a non-linear (NL) layer under the anodic side. The different shape of the MF patterns obtained for the two studied compositions can be attributed to the difference of the thickness of the NL layer and might be related to a higher ionic character in $50GeS_2$–$20In_2S_3$–30CsI compared to $70GeS_2$–$20In_2S_3$–10CsI glass network. The MF shape of $50GeS_2$–$20In_2S_3$–30CsI glass is the mark of a NL layer thickness lower than the coherent length L_c ($L_c = \lambda_\omega/[4(n_{2\omega} - n_\omega)]$), which is about 15 μm in these materials, whereas the NL layer thickness may be higher for the $70GeS_2$–$20In_2S_3$–10CsI glass which could explain the observation of several fringes or overmodulations in the latter case. Several mechanisms could be considered to explain the creation of a non-linearity, such as the migration of mobile cations, like Na^+, K^+ etc. Underneath the anode, a layer of a few microns becomes depleted of cations, whereas a thin layer acquires an excess of cations underneath the cathode. It is also known that in alkali rich glasses, alkali ions can physically come out of the sample and a white oxide deposit is observed on the cathode side [27]. This accumulation of negative charges leads to the creation of a high internal electric field E_{dc} near the anodic side resulting in the creation of SHG through the contribution of the term $\chi^{(3)}E_{dc}$. This mechanism could be followed by the reorientation of electrical dipoles or hyperpolarizable entities – as the sulfur lone pairs – under the induced electric field E_{dc}. The relatively high ionic and electronic conductivities could explain the spontaneous decay of the SHS caused by the relaxation of the space charge induced during the poling [28].

5. Conclusion

A large glass-forming region was found in the GeS_2–In_2S_3–CsI system. NL optical and physical properties have been studied. The introduction of cesium iodide results in a decrease of the dimensionality of the In_2S_3–GeS_2 covalent network. These glasses present NL refractive index n_2 than 60 times higher than silica glasses without any NL absorption. SHG was observed in thermally poled samples; however, this second order non-linearity was not temporally stable.

References

[1] A. Turnbull, J.S. Sanghera, V.Q. Nguyen, I.D. Aggarwal, Mater. Lett. 58 (12) (2004) 51.
[2] A. Zakery, S.R. Elliott, J. Non-Cryst. Solids 330 (1–3) (2003) 1.
[3] C. Quemard, F. Smektala, V. Couderc, A. Barthelemy, J. Lucas, Phys. Chem. Soc. 73 (6) (1999) 1794.
[4] J.S. Sanghera, J. Heo, J.D. Mackenzie, J. Non-Cryst. Solids 103 (1988) 155.
[5] J. Heo, J.D. Mackenzie, J. Non-Cryst. Solids 111 (1989) 29.
[6] D. Marchese, G. Kakarantzas, A. Jha, B.N. Samson, J. Wang, J. Mod. Opt. 43 (1996) 963.
[7] Yu.S. Tver'yanovich, E.G. Nedoshovenko, V.V. Aleksandrov, E. Yu. Turkina, A.S. Tver'yanovich, I.A. Sokolov, Glass. Phys. Chem. 22 (1996) 963.
[8] J. Le Person, V. Nazabal, J.L. Adam, Solid State Sci. 7 (2005) 303.
[9] H. Tao, S. Mao, W. Tong, X. Zhao, Mater. Lett. 60 (2006) 741.
[10] S. Mao, H.Z. Tao, X.J. Zhao, G.P. Dong, H.T. Guo, Solid State Commun. 142 (2007) 453.
[11] Z. Boncheva–Mladenova, Z.G. Ivanova, J. Non-Cryst. Solids 30 (1978) 147.
[12] R. Todorov, T. Iliev, K. Petkov, J. Non-Cryst Solids 326-327 (2003) 263.
[13] M. Bilkova, P. Nemec, M. Frumar, J. Optelectron. Adv. Mater. 7 (2005) 2247.
[14] S. Sen, B.G. Aitken, S. Khalid, J. Non-Cryst. Solids 351 (2005) 1710.
[15] H. Tao, S. Mao, G. Dong, H. Xiao, X. Zhao, Solid State Commun. 137 (2006) 408.
[16] M. Repkova, P. Nemec, M. Frumar, J. Optoelectron. and Adv. Mater. 8 (2006) 1796.
[17] P.D. Maker, R.W. Terhune, M. Nisenoff, C.M. Savage, Phys. Rev. Lett. 8 (1) (1962) 21.
[18] R. Suker, R.W. Gammon, Phys. Rev. Lett. 25 (1970) 222.
[19] G. Lucovsky, F.L. Galeener, R.C. Keezer, R.H. Geils, H.A. Six, Phys. Rev. B 10 (1974) 5134.
[20] J. Heo, J.D. Mackenzie, J. Non-Cryst. Solids 113 (1989) 246.
[21] A.M. Loireau-Lozac'h, F. Keller-Besrest, S. Benazeth, J. Solid State Chem. 123 (1996) 60.
[22] K. Kambas, J. Spyridelis, M. Balkanski, Phys. Status Solidi (b) 105 (1981) 291.
[23] L. Koudelka, M. Pisarcik, J. Non-Cryst. Solids 113 (1989) 239.
[24] M.J. Taylor, L.A. Klo, J. Raman Spectrosc. 31 (2000) 465.
[25] S.D. Ross, Inorganic Infrared and Raman Spectra, McGraw-Hill, London, 1972, p. 200.
[26] M. Guignard, V. Nazabal, F. Smektala, H. Zeghlache, A. Kudlinski, Y. Quiquempois, G. Martinelli, Optics Express 14 (2006) 1524.
[27] D.E. Carlson, K.W. Hang, G.F. Stockdale, J. Am. Ceram. Soc. 55 (1972) 337.
[28] Z. Ivanova, J. Non-Cryst. Solids 90 (1987) 569.